nature astronomy

LETTERS

https://doi.org/10.1038/s41550-019-0915-8

A basin-free spherical shape as an outcome of a giant impact on asteroid Hygiea

P. Vernazza[1*], L. Jorda[1], P. Ševeček[2], M. Brož[2], M. Viikinkoski[3], J. Hanuš[2], B. Carry[4], A. Drouard[1], M. Ferrais[5], M. Marsset[6], F. Marchis[1,7], M. Birlan[8], E. Podlewska-Gaca[9,10], E. Jehin[5], P. Bartczak[9], G. Dudzinski[9], J. Berthier[8], J. Castillo-Rogez[11], F. Cipriani[12], F. Colas[8], F. DeMeo[6], C. Dumas[13], J. Durech[2], R. Fetick[1,14], T. Fusco[1,14], J. Grice[4,15], M. Kaasalainen[3], A. Kryszczynska[9], P. Lamy[1], H. Le Coroller[1], A. Marciniak[9], T. Michalowski[9], P. Michel[4], N. Rambaux[8], T. Santana-Ros[16,17], P. Tanga[4], F. Vachier[8], A. Vigan[1], O. Witasse[12], B. Yang[18], M. Gillon[5], Z. Benkhaldoun[19], R. Szakats[20], R. Hirsch[9], R. Duffard[21], A. Chapman[22] and J. L. Maestre[23]

(10) Hygiea is the fourth largest main belt asteroid and the only known asteroid whose surface composition appears similar to that of the dwarf planet (1) Ceres[1,2], suggesting a similar origin for these two objects. Hygiea suffered a giant impact more than 2 Gyr ago[3] that is at the origin of one of the largest asteroid families. However, Hygeia has never been observed with sufficiently high resolution to resolve the details of its surface or to constrain its size and shape. Here, we report high-angular-resolution imaging observations of Hygiea with the VLT/SPHERE instrument (~20 mas at 600 nm) that reveal a basin-free nearly spherical shape with a volume-equivalent radius of 217 ± 7 km, implying a density of 1,944 ± 250 kg m^{-3} to 1σ. In addition, we have determined a new rotation period for Hygiea of ~13.8 h, which is half the currently accepted value. Numerical simulations of the family-forming event show that Hygiea's spherical shape and family can be explained by a collision with a large projectile (diameter ~75–150 km). By comparing Hygiea's sphericity with that of other Solar System objects, it appears that Hygiea is nearly as spherical as Ceres, opening up the possibility for this object to be reclassified as a dwarf planet.

Although it is an easy target for ground-based observations owing to its large angular diameter, Hygiea is the least studied of the four asteroids with diameters greater than 400 km (Ceres, (2) Pallas, (4) Vesta and Hygiea; Fig. 1), whose large sizes may have allowed them to reach hydrostatic equilibrium early in their history. It follows that a number of its basic physical properties, such as its shape and spin state, have not yet been reliably constrained.

To constrain these physical properties, we performed—as part of our European Southern Observatory large programme[4]—high-angular-resolution imaging observations of Hygiea with the SPHERE (Spectro-Polarimetric High-contrast Exoplanet REsearch) instrument on the VLT (Very Large Telescope) at 12 different epochs in 2017 and 2018. We used the new-generation visible adaptive optics ZIMPOL (Zurich IMaging POLarimeter)[5] in narrow-band imaging mode (N_R filter; central wavelength 645.9 nm). To restore the optimal angular resolution of each reduced image, we used the MISTRAL (Myopic Iterative STep Preserving ALgorithm) myopic deconvolution algorithm[6] along with a parametric point spread function[7]. We then applied the All-Data Asteroid Modeling (ADAM)[8] algorithm to our set of deconvolved images to reconstruct the three-dimensional (3D) shape model and the spin of Hygiea. The shape reconstruction was complicated by discernible albedo variegation apparent in the images (see Methods). To take into account such phenomena, the relative brightness of each facet with respect to the surrounding ones was treated as a free parameter (we allowed a maximum variegation of ±30%), and we further defined a smoothing operator as a regularization term to prevent large deviations between neighbouring facets. The comparison between the 12 adaptive optics epochs and the corresponding shape model projections is shown in Fig. 2.

Our best fits yielded semi-axes of 225 ± 5 km, 215 ± 5 km and 212 ± 10 km and a volume-equivalent radius of 217 ± 7 km. We found a rotational pole of right ascension 319 ± 3°, declination −46 ± 3° and a rotation period of 13.82559 ± 0.00005 h, which is half the previously reported and widely accepted value[9]. Our rotation period is compatible both with all light curves acquired so far for Hygiea, including the ones acquired with the Transiting Planets and Planetesimals Small Telescopes (TRAPPIST) in parallel with

[1]LAM (Laboratoire d'Astrophysique de Marseille) UMR 7326, Aix Marseille Université, CNRS, Marseille, France. [2]Institute of Astronomy, Charles University, Prague, Czech Republic. [3]Mathematics and Statistics, Tampere University, Tampere, Finland. [4]Laboratoire Lagrange, Université Côte d'Azur, Observatoire de la Côte d'Azur, CNRS, Nice, France. [5]Space Sciences, Technologies and Astrophysics Research Institute, Université de Liège, Liège, Belgium. [6]Department of Earth, Atmospheric and Planetary Sciences, MIT, Cambridge, MA, USA. [7]SETI Institute, Carl Sagan Center, Mountain View, CA, USA. [8]IMCCE, Observatoire de Paris, Paris, France. [9]Astronomical Observatory Institute, Faculty of Physics, Adam Mickiewicz University, Poznań, Poland. [10]Institute of Physics, University of Szczecin, Szczecin, Poland. [11]Jet Propulsion Laboratory, California Institute of Technology, Pasadena, CA, USA. [12]European Space Agency, ESTEC - Scientific Support Office, Noordwijk, the Netherlands. [13]TMT Observatory, Pasadena, CA, USA. [14]ONERA, The French Aerospace Lab, Chatillon, France. [15]School of Physical Sciences, The Open University, Milton Keynes, UK. [16]Departamento de Física, Ingeniería de Sistemas y Teoría de la Señal, Universidad de Alicante, Alicante, Spain. [17]Institut de Ciències del Cosmos, Universitat de Barcelona, Barcelona, Spain. [18]European Southern Observatory (ESO), Santiago, Chile. [19]Oukaimeden Observatory, High Energy Physics and Astrophysics Laboratory, Cadi Ayyad University, Marrakesh, Morocco. [20]Konkoly Observatory, Research Centre for Astronomy and Earth Sciences, Hungarian Academy of Sciences, Budapest, Hungary. [21]Instituto de Astrofísica de Andalucía (CSIC), Glorieta de la Astronomía, Granada, Spain. [22]Observatorio de Buenos Aires, Buenos Aires, Argentina. [23]Observatorio de Albox, Albox, Spain. *e-mail: pierre.vernazza@lam.fr

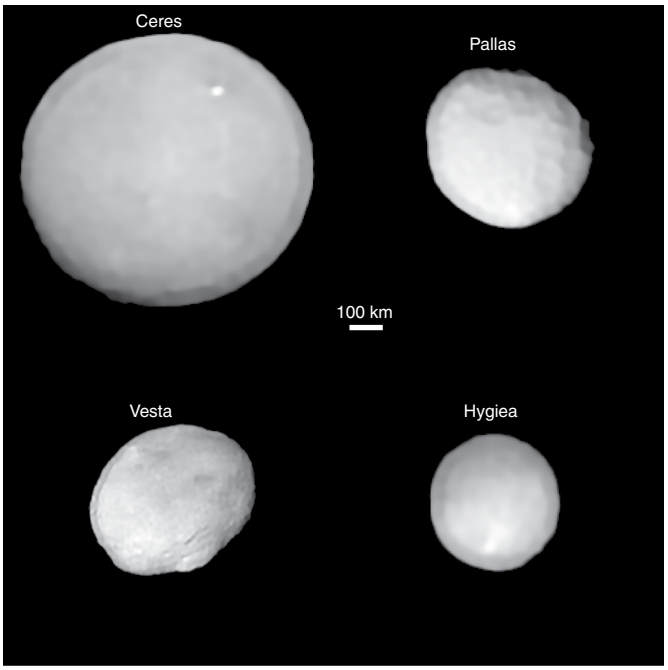

Fig. 1 | VLT/SPHERE deconvolved images of the four largest main belt objects. The relative sizes are respected, and the scale is indicated on the plot.

our SPHERE observations (Supplementary Fig. 1), and the SPHERE images. The axial ratios, including their uncertainties, appear compatible with the equilibrium Maclaurin spheroid. The specific angular momentum $L_{norm} = L/\sqrt{GM^3R}$, where L denotes the actual angular momentum of the body, G the gravitational constant, M the mass and R the mean radius, is equal to 0.070 ± 0.002, which is lower than the bifurcation point (0.304) where the equilibrium figure becomes a triaxial Jacobi ellipsoid[10].

Our shape and our best estimate of Hygiea's mass ($(8.32 \pm 0.80) \times 10^{19}$ kg; Supplementary Fig. 2 and Supplementary Table 3) yield a density of 1,944 ± 250 kg m^{-3}. Such density is compatible, within errors, with Ceres's density[11] (2,161.6 ± 2.5 kg m^{-3}). Note that the reaccumulation process following the giant impact at the origin of the family may have triggered some level of macroporosity, and the original density of Hygiea may be even closer to that of Ceres. The high water fraction inferred in both cases, along with their similar spectral properties[1,2], imply a formation location beyond the snowline for these two bodies.

We observed Hygiea with sub-Earth latitudes near 50° S (first epoch) and 24° S (second epoch) so that the visible surface extended from 66° N to 90° S, leading to ~95% surface coverage. Surprisingly, none of our images and their associated contours (Supplementary Fig. 3) revealed the large impact basin expected from the large size of the Hygiea family[3,12] (volume-equivalent diameter (D_{eq}) of the family members ~100 km; see Methods). In comparison, Vesta possesses a large impact basin that is clearly observable from the ground[7,13] (Fig. 1), although its family is smaller in volume than Hygiea's family by a factor of ~8 ($D_{eq} \approx 50$ km)[12]. To quantify the overall absence of a large basin on Hygiea, we fit Hygiea's 3D shape model with an ellipsoid and, subsequently, measured the radial difference between the two shapes. We also calculated the volume fraction of excavated material as $|V_{body} - V_{ellipsoid}|/V_{body}$. We performed the same calculations for Ceres and Vesta. Our calculations show that the large-scale topography of Hygiea is similar to that of Ceres, implying a global lack of large impact basins across its surface. They also reveal that—similar to Ceres—Hygiea's shape is very close to that of an ellipsoid. In the case of Vesta, the existence of a large depression is clearly observed in the histogram (Supplementary Fig. 4).

To investigate the origin of Hygiea's nearly spherical shape, as well as the absence of a large impact basin, we used a smoothed-particle hydrodynamics (SPH) code[14–16] to simulate the family-forming event. Our code is well adapted to simulate collisions of rotating and self-gravitating asteroids. We assumed monolithic basaltic material, the Tillotson equation of state[17], the von Mises yield criterion[18] to account for plastic deformations and the Grady–Kipp model[19] for fragmentation. The self-gravity has been implemented using the Barnes–Hut algorithm[20]. All input parameters are listed in Supplementary Table 5. Before running the simulations, our code was tested against previous studies[14], and we carefully verified the stability of rotating objects, as well as the validity of the gravity approximation by comparing it with the 'brute force' approach.

We performed a large number of simulations testing various projectile diameters (D_{imp} range: 70–150 km), impact angles (ϕ_{imp} range: 15–60°) and initial rotation periods for the target (P_{pb} range: 3–∞ h, where the subscript 'pb' denotes the parent body). Large values for the projectile diameter were required to match the large size of the Hygiea family. We further used a range of impact speeds from 5 km s^{-1} to 7 km s^{-1}. Both fragmentation and reaccumulation phases were computed by the SPH algorithm to resolve the shape of the largest remnant (that is, Hygiea). For the final reaccumulation only, we switched to a more efficient N-body algorithm, using hard-sphere and perfect-merging approximations, to obtain a synthetic family and its size-frequency distribution (SFD). The numerical model is described in detail in Methods.

A first outcome of our simulations is that Hygiea's final shape is highly spherical, regardless of the diameter of the impactor (in the 75–150 km size range) and the impact angle (Fig. 3). In particular, all pre-existing surface features have been erased, implying that the observed absence of a large impact basin on Hygiea is a natural outcome of the family-forming impact. We further used the SFD of the observed family to better constrain the parameters of the giant collision. It appears that the observed SFD can be matched either by head-on (0–30°) $D_{imp} = 75$ km impacts or, alternatively, oblique (30–60°) $D_{imp} = 150$ km impacts, although only the head-on impacts form one or a few intermediate-sized (40 km < D < 100 km, where D is the diameter) fragments; no such fragments are formed for impact angles greater than 45°. Given that the second largest body of the family ((1599) Giomus; see Methods) is indeed an intermediate-sized fragment, the head-on impact is more plausible. It follows that the impactor probably had $D_{imp} \approx 100$ km. Our simulations imply that the impact fully damaged the parent body and resulted in substantial reaccumulation[21]. When Hygiea formed, macroscopic oscillations drove the material to behave as a fluid[22], naturally resulting in the formation of a nearly spherical object in rotational equilibrium (Fig. 3). Accordingly, the effective friction of the damaged material had to be negligible for Hygiea (see Methods). Some departures from a rotational equilibrium can occur only if the material regains its strength, for example when acoustic fluidization is stopped[23,24]. Indeed, we detect global oscillations of the shape in our simulations (see Supplementary Fig. 5), which logically occur on the Keplerian timescale, that is, 2.4 h. Using a, b and c for semi-axes of a dynamically equivalent ellipsoid, we can explain the observed b/a and c/b ratios provided the fluidization stopped after approximately 4 h. In contrast to Hygiea, the Rheasilvia basin on Vesta resulted from an impact by a $D \approx 65$ km-sized projectile[25]. In this case, we suppose that, as Vesta is around three times more massive than Hygeia, the impact energy was not sufficient to completely shatter it, and the collision ended up being an excavation event.

The nearly spherical shape of Hygiea led us to evaluate the possibility of classifying this object as a dwarf planet. Any main belt asteroid immediately satisfies three of the four characteristics required for an object being labelled a dwarf planet, namely, a celestial

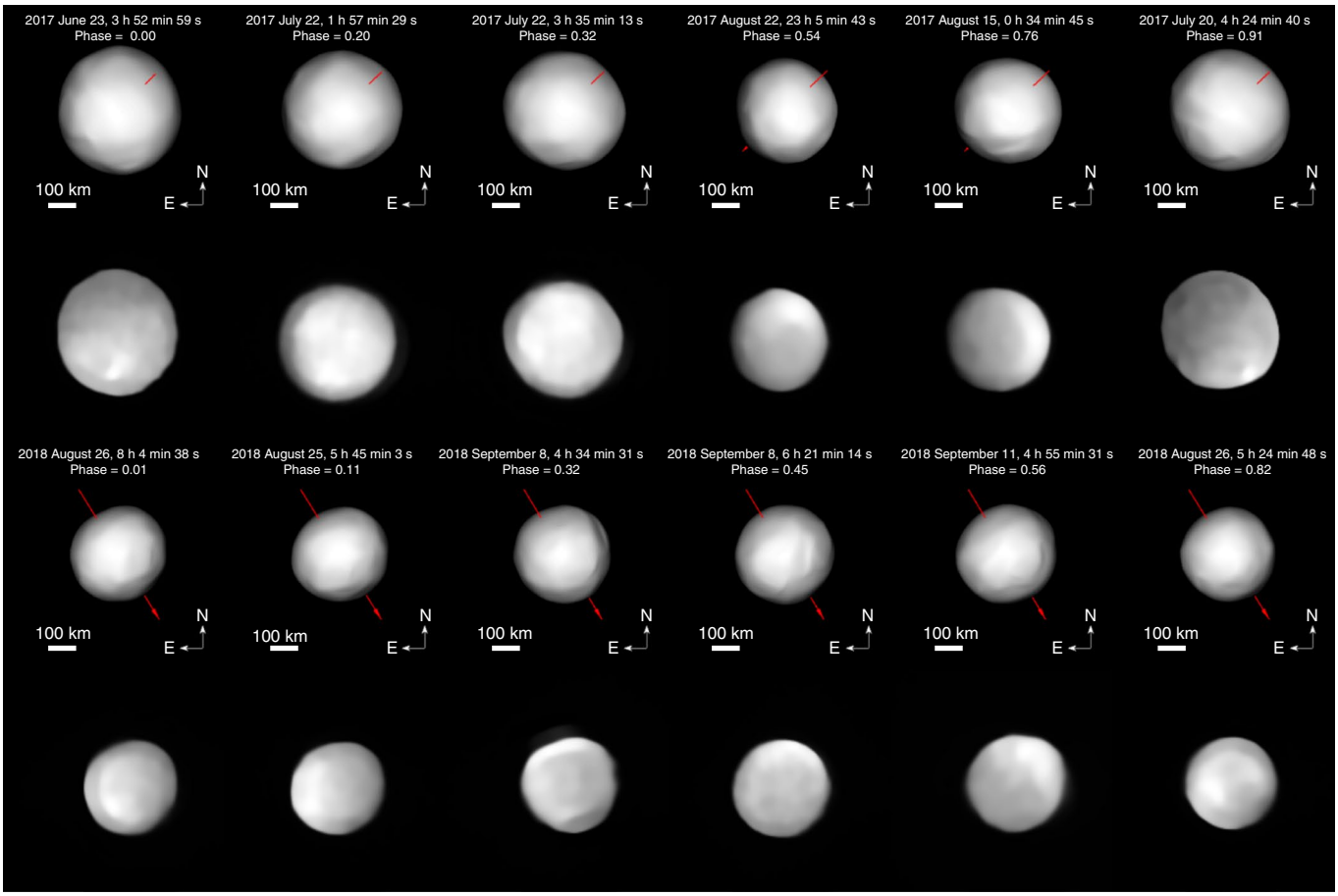

Fig. 2 | Comparison between the deconvolved images of Hygiea and the corresponding shape model projections. Bottom rows: Hygiea. Top rows: the corresponding shape model projections. Hygiea's spin axis (red) is also shown.

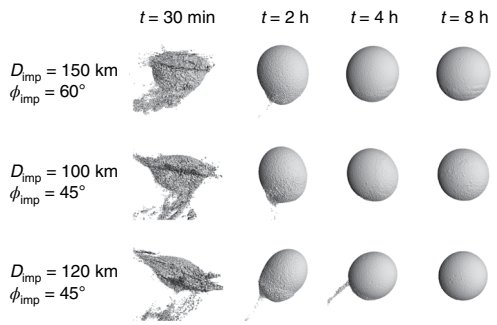

Fig. 3 | SPH simulations reveal a nearly spherical shape for Hygiea following post-impact reaccumulation. SPH simulations were ran to simulate the giant collision at the origin of the prominent Hygiea family, with a focus on the post-impact shape of the largest remnant, namely, Hygiea. For an accurate representation of the surface, we generated it as an isosurface of the density, using the ray-marching algorithm, rather than rendering individual SPH particles. At time $t = 30$ min, Hygiea is fully fragmented and notably deformed. Shortly after, most of the ejected material reaccumulates on Hygiea. Finally, macroscopic oscillations are suppressed, and Hygiea reaches a nearly spherical equilibrium shape. No large crater has been preserved.

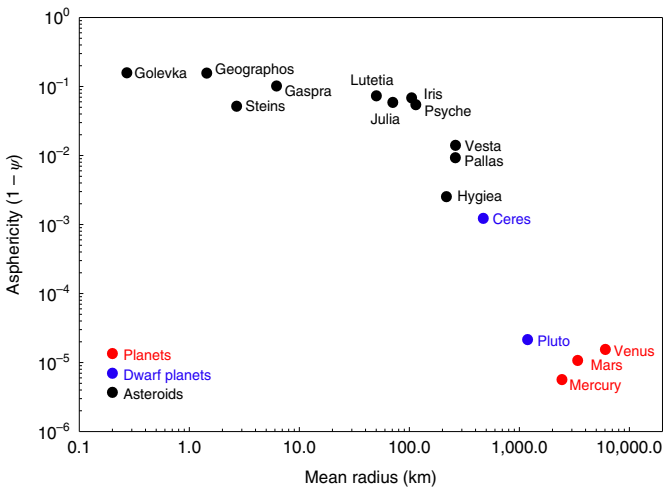

Fig. 4 | Asphericity of Solar System objects as a function of their mean radius. The parameter ψ corresponds to the sphericity index[26] applied to spherical harmonics developments of the 3D shape models of each object. Hygiea appears nearly as spherical as the dwarf planet Ceres.

body that (1) is in orbit around the Sun, (2) has not cleared the neighbourhood around its orbit and (3) is not a satellite. The fourth requirement is to have sufficient mass for its self-gravity to overcome rigid body forces so that it assumes a hydrostatic equilibrium nearly round shape. To properly quantify this last and essentially main criterion, we measured the sphericity[26], ψ, of Hygiea (see Methods) for comparison with that of the terrestrial planets, the two dwarf planets (134340) Pluto and Ceres and a few asteroids (Fig. 4).

It appears that Hygiea is nearly as spherical as Ceres ($\psi_{\text{Hygiea}} \approx 0.9975$; $\psi_{\text{Ceres}} \approx 0.9988$). Hygiea could thus be classified as a dwarf planet, so far the smallest in the Solar System. We anticipate the discovery of several new dwarf planet candidates when 3D shape models become available for $D > 400$ km trans-Neptunian objects.

Methods

Revision of Hygiea's rotation period. As part of our European Southern Observatory large programme[4] (199.C-0074; principal investigator: P.V.), we acquire complementary light curves when the pole solution of our target is not well constrained and/or when we are not able to reconstruct its 3D shape with ADAM[8], possibly indicating a wrong estimate of its pole solution or of its rotation period. This is exactly the case for Hygiea. Since 1991[9], multiple authors have all reported a rotation period of 27.6 h for Hygiea[27], but there has always been a lack of densely sampled phased light curves for this object.

We therefore planned our observations assuming a 27.6 h rotation period, and we observed Hygiea with TRAPPIST-North and -South[28] over a time frame of ~40 nights. The phased light curve started to show an ordinary double-sinusoidal shape as our observations were going on. However, the light curve appeared to be perfectly symmetrical, which is very unlikely. We then phased the data using the half period of ~13.8 h, which produced a very convincing fit with a single peak light curve (Supplementary Fig. 1). Assuming this new rotation period, we were able to reconstruct Hygiea's 3D shape model and to constrain its spin. In addition, the phasing of our VLT/SPHERE images acquired at several epochs were correct with this new rotation period, which was not the case with the old one.

How round is Hygiea?. *Contour extraction.* We used a first approach, namely, contour extraction[7], to highlight the sphericity of Hygiea. In Supplementary Fig. 3, we compare the contours of our Hygiea images with those of a sphere, revealing—on average—a minimal difference between the two. It is important to stress that the contours obtained with VLT/SPHERE are precise at the pixel level[7].

Calculation of the sphericity. To constrain Hygiea's sphericity and compare it with that of other Solar System bodies, including planets and minor bodies (asteroids, comets), we applied a sphericity formula[26] to our 3D shape model. Following this formula, the sphericity is a function of the surface area and of the volume. However, the surface area is very sensitive to the surface topography and the resolution of the 3D shape model. Therefore, performing a direct comparison of the sphericity of various objects having very different 3D shape model resolutions and/or topographies would lead to incorrect results. To overcome this problem and to perform a self-consistent comparison, we computed the real spherical harmonic expansion coefficients (tenth order) of the 3D shape model for each object[4,29–40]. By doing so, we produced 3D shape models that reproduce well the overall shape of our objects, ignoring the small-scale topographic variations. An example of the procedure is highlighted in Supplementary Fig. 6. As a final step, we applied the formula of the sphericity to these spherical harmonics models.

Hygiea's reflectance map. The best-quality SPHERE images were combined into a cylindrical-projection map to study the main geological features of Hygiea. We call it a reflectance map because it contains both albedo and shadow information. Indeed, the limited number of observed geometries and the resolution of the images do not allow us to accurately correct for illumination of local topography. As a consequence, we cannot always separate albedo information from shadowing effects.

The quality of each sequence of observations was evaluated according to three criteria: (1) the angular size of Hygiea at the time of the observation, (2) the presence, or not, of deconvolution artefacts in the images and (3) the consistency of the location of the main albedo features on the surface of Hygiea across the full sequence of images. According to these criteria, the first two epochs of observations, 2017 June 23 and 2017 July 20, were found to provide the highest image quality. The images for these two epochs also exhibit the highest variability in reflectance seen across the surface of Hygiea, and include most of its main albedo features. We therefore chose to use only these images to maximize the resolution and reliability of our map, despite the fact that they sample only about one-third of the total surface covered by our complete set of observations.

A photometric correction was applied to each image to correct the overall illumination gradient[7]. The asteroid-centric longitude and latitude of each pixel were measured using the ADAM shape model, and the values were projected using an equidistant cylindrical projection. The individual maps built from the complete set of selected images were then combined, using their overlapping regions to adjust their brightness level[7]. The combined map was finally normalized to the average geometric albedo of Hygiea of 7.2%.

The resulting reflectance map is shown in Supplementary Fig. 7. It exhibits a wide range of values, with more than 20% variability with respect to the average, although shadowed regions enhance this variability. Several bright spots are clearly identifiable, the brightest one, located near longitude $\lambda = 290°$, latitude $\phi = -30°$, showing a 10% brightness enhancement with respect to the average reflectance. The large dark region at $\lambda = 60°$, $\phi = 0°$ is most probably a shadowed region, as it is located near the asteroid limb on the second sequence of images.

For comparison, we further show a reflectance map of Ceres (Supplementary Fig. 7), built from our SPHERE observations following the same method as described above for Hygiea. Ceres was observed at one epoch as the benchmark target for our observing programme, with the NASA Dawn mission providing us with the ground truth for that object. Similarly to Hygiea, we used only the best-quality image acquired for that object when building its map. This image contains Ceres's main albedo feature, the bright spot located in the Occator crater. Ceres is slightly brighter than Hygiea in average albedo ($p_V = 0.09$ versus $p_V = 0.07$, where p_V is geometric albedo in the visual (V) band). The range of reflectance values revealed by our observations for these two bodies is very similar, with about 20% variability. Ceres's bright spot in the Occator crater, located around $\lambda = 240°$, $\phi = 20°$, shows a 20% brightness enhancement with respect to Ceres's average. To conclude, like the density and the spectral properties, the reflectance/albedo properties of Hygiea and Ceres are highly similar.

Cratering on Hygiea. From our set of images, we could identify only two unambiguous craters, with respective diameters of 180 ± 15 km and 97 ± 10 km (Supplementary Fig. 8). This low number of identified craters contrasts with the large number of craters recognized at the surface of Pallas (Fig. 1) and that of Vesta[7] and (7) Iris[41]. Although this may be understood as Hygiea's surface being younger than that of the above-mentioned bodies, it is unlikely to be the only explanation, given that Hygiea's surface age (estimated formation time of the family) is estimated to be at least 3 Gyr (ref. [3]). Both the crater morphology and, to a lesser extent, the reflectance properties of the surface play an important role in the contrast between the crater rim and crater floor. Whereas bowl-shaped craters will be easily identifiable from the ground, leading to a clear contrast between the crater floor/walls and the crater rim, the same will not be true in the case of complex craters with a flat floor. Most probably, our observations imply a paucity of large ($D > 30$ km, which corresponds to our detection limit) bowl-shaped craters in the case of Hygiea. This is an additional common feature between Hygiea and Ceres. In the case of Ceres, the Dawn mission has unambiguously revealed a heavily cratered surface[42], where most $D > 10$–15 km craters are not bowl shaped, but flat floored. By analogy with Ceres, this strongly supports the presence of water ice in the subsurface of Hygiea. The presence of water ice in the subsurface would also favour the relaxation of the surface topography as observed on Ceres[43], thus rendering the remote-sensing identification of craters on Hygiea more difficult.

Identifying the members of the Hygiea family. Before running the SPH simulations, we carefully identified the Hygiea family members using the proper elements[44] and the hierarchical clustering method[45], with the cut-off relative velocity $v_{\text{cut}} = 60\ \text{m s}^{-1}$. We further used physical data to remove interlopers with incompatible spectra (Supplementary Fig. 9 and Supplementary Table 4), colour (using Sloan Digital Sky Survey data[46]) or albedo (using Wide-field Infrared Survey Explorer[47] and AKARI[48] data). We found 6,857 family members and constructed their SFD. Besides the usual largest remnant (Hygiea), there is one intermediate-sized asteroid, namely Giomus, with $D = 46$ km, whose near-infrared spectrum is compatible with that of Hygiea (Supplementary Fig. 9). By summing the masses of fragments, we estimate that the mass ejected during the collision is at least 1.7% of the mass of Hygiea. In comparison, the ejected mass of the Vesta family makes up only 0.5% of Vesta, suggesting that the Hygiea-forming impact was substantially more energetic.

Numerical model. Impact simulations have been carried out using our SPH/*N*-body code OpenSPH. The code can perform both SPH and *N*-body simulations. It thus allows us to run a whole simulation, from an initial fragmentation to a final reaccumulation. In all simulations presented here, the duration of the SPH simulation is $t_{\text{SPH}} = 24$ h, which is sufficient for the largest remnant (as well as for the largest fragments) to gain a well-defined shape and damp any macroscopic oscillations. We then follow up with the *N*-body simulation for another $t_{N\text{-body}} = 10$ d to obtain the final SFD of the synthetic family. The hand-off between the SPH and *N*-body parts is done by simply changing the solver and modifying the particle radii, $R_i = [3M_i/(4\pi\rho)]^{1/3}$, where M_i and R_i are respectively the mass and the radius of the ith particle, and ρ is the material density of the particle, to convert smoothed particles into hard spheres while preserving their masses and volumes.

The SPH solver computes particle accelerations due to the stress tensor and self-gravity, shock heating, material yielding and fragmentation. It further includes the artificial viscosity term for proper treatment of shocks, the artificial stress to suppress tensile instabilities and the correction tensor for consistent bulk rotation[49]. The code can use either a frictionless rheology (von Mises criterion) or a more complex Drucker–Prager rheology[15,50], which includes both internal friction for intact material and dry friction for damaged material. Motivated by the observed round shape of Hygiea, we used the simpler frictionless model, as the friction clearly did not play a major role in the Hygiea-forming impact. For comparison, we also ran simulations with various friction coefficients.

During *N*-body simulations, we searched for particle collisions, performing either an inelastic bounce or a merging of collided particles, depending on their relative velocities and the spin rate of the merger. When particles merged, the

resulting volume, velocity and spin rate of the merger were determined, to conserve the total volume, momentum and angular momentum. Overlapping particles were treated the same way as collided particles; as we performed a late hand-off when the relative velocities of particles inside individual fragments were already small, the respective particles underwent a quick merging, and a precise handling of overlaps was not needed. Although merging erased the shape information, here, we are interested only in fragment sizes, and merging is thus a viable option.

Rheology in SPH simulations. In the simulations presented in the main text, we use the von Mises criterion. The yield stress is computed using $Y=(1-d)Y_m$, where Y_m is a material-specific, but pressure-independent, constant and d is the scalar damage. In this model, fully damaged material experiences no friction and essentially behaves as a fluid.

To model friction of granular material (which would be especially important for asteroids and impacts much smaller than in Hygiea's case), we also implemented the Drucker–Prager rheology[15,50] in our code. It defines the yield strength of intact material as

$$Y_i = Y_0 + \frac{\mu_i p}{1+\mu_i p/(Y_{vM}-Y_0)}$$

where μ_i is the coefficient of internal friction, Y_0 is the cohesion (yield strength at zero pressure), Y_m is the von Mises elasticity limit and p is the pressure. For fully damaged rock, the yield strength, Y_d, is proportional to the pressure as $Y_d=\mu_d p$, where μ_d is the coefficient of dry friction, which is related to the angle of repose. In the intermediate state where $0<d<1$, the yield strength is given by a linear interpolation, $Y=(1-d)Y_i+dY_d$.

The final shape of the largest remnant is affected by the coefficient of dry friction. However, using the model with non-negligible friction, $\mu_d>0.1$, yields a very poor match to the observed round shape of Hygiea (see Supplementary Fig. 10). This issue has been previously recognized by studies of cratering events[24,25] and is commonly explained by introducing the acoustic fluidization. In the block model of acoustic fluidization, yield strength is further modified as $Y_{vib}=\mu_d(p-p_{vib})+\eta_l\rho\dot{\epsilon}$, where p_{vib} is the vibrational pressure, calculated from the maximum vibrational particle velocity[51], η_l is the effective viscosity of fluidized material and $\dot{\epsilon}$ is the strain rate. The vibrational velocity is exponentially attenuated after the impact; however, the timescale of this process is a free parameter. Instead of using the block model directly, we prefer the von Mises model, with a similar free parameter, that is, the timescale of acoustic fluidization after which the body regains its strength. This model matches the observed shape very well (see Fig. 3 and Supplementary Fig. 10).

Parameters of the SPH simulations. We considered both the target and the impactor to be monolithic bodies with an initial density of the material $\rho_0=2{,}000\,\mathrm{kg\,m^{-3}}$, corresponding to the present-day density of Hygiea. We assumed material properties of basalt[14,16]. The pressure and the sound speed were determined using the Tillotson equation of state, assuming bulk modulus $A=2.67\times10^{10}$ Pa, and specific energies for incipient and complete vaporization $u_{iv}=4.72\times10^6\,\mathrm{J\,kg^{-1}}$ and $u_{cv}=1.82\times10^7\,\mathrm{J\,kg^{-1}}$, respectively. The strength model used the von Mises yield criterion with shear modulus $\mu=2.27\times10^{10}$ Pa, elasticity limit $Y_m=3.5\times10^9$ Pa and specific melting energy $u_{melt}=3.4\times10^6\,\mathrm{J\,kg^{-1}}$. To account for material fragmentation, we used the Grady–Kipp model with Weibull coefficient $k=4\times10^{29}$ and Weibull exponent $m=9$. In our simulations, the target had $N\approx4\times10^5$ particles, the spatial resolution therefore being ~6 km, which is sufficient to resolve hundreds of the family members. The number of particles for the impactor was chosen so as to obtain the same particle density as the target. The equations were integrated using a predictor–corrector method, the time step of which was limited by the Courant–Friedrichs–Lewy criterion with Courant number $C=0.2$. A subset of our simulations and the parameters used are displayed in Supplementary Fig. 5. Finally, the cumulative SFDs of synthetic families are compared with the SFD of the observed Hygiea family in Supplementary Fig. 11.

Data availability

As soon as papers for our large programme are accepted for publication, we will make the corresponding reduced and deconvolved adaptive optics images and 3D shape models publicly available at http://observations.lam.fr/astero/.

Code availability

The code used to generate the 3D shape is freely available at https://github.com/matvii/ADAM. The code used to perform the SPH simulations is freely available at https://gitlab.com/sevecekp/sph.

Received: 8 April 2019; Accepted: 13 September 2019;
Published online: 28 October 2019

References

1. Takir, D. & Emery, J. P. Outer main belt asteroids: identification and distribution of four 3-μm spectral groups. *Icarus* **219**, 641–654 (2012).
2. Vernazza, P. et al. Different origins or different evolutions? Decoding the spectral diversity among C-type asteroids. *Astron. J.* **153**, 72 (2017).
3. Carruba, V., Domingos, R. C., Huaman, M. E., dos Santos, C. R. & Souami, D. Dynamical evolution and chronology of the Hygiea asteroid family. *Mon. Not. R. Astron. Soc.* **437**, 2279–2290 (2014).
4. Vernazza, P. et al. The impact crater at the origin of the Julia family detected with VLT/SPHERE? *Astron. Astrophys.* **618**, A154 (2018).
5. Thalmann, C. et al. SPHERE ZIMPOL: overview and performance simulation. *Proc. SPIE* **7014**, 70143F (2008).
6. Fusco, T. et al. Deconvolution of astronomical images obtained from ground-based telescopes with adaptive optics. *Proc. SPIE* **4839**, 1065–1075 (2003).
7. Fetick, R. et al. Closing the gap between Earth-based and interplanetary mission observations: Vesta seen by VLT/SPHERE. *Astron. Astrophys.* **623**, A6 (2019).
8. Viikinkoski, M., Kaasalainen, M. & Durech, J. ADAM: a general method for using various data types in asteroid reconstruction. *Astron. Astrophys.* **576**, A8 (2015).
9. Michalowski, T. et al. The spin vector of asteroid 10 Hygiea. *Astron. Astrophys. Suppl. Ser.* **91**, 53–59 (1991).
10. Chandrasekhar, R. *Ellipsoidal Figures of Equilibrium* (Dover Publications, 1987).
11. Park, R. S. et al. High-resolution shape model of Ceres from stereophotoclinometry using Dawn imaging data. *Icarus* **319**, 812–827 (2019).
12. Nesvorný, D., Brož, M. & Carruba, V. in *Asteroids IV* (eds Michel, P. et al.) 297–321 (Univ. Arizona Press, 2015).
13. Thomas, P. C. et al. Impact excavation on asteroid 4 Vesta: Hubble Space Telescope results. *Science* **277**, 1492–1495 (1997).
14. Benz, W. & Asphaug, E. Impact simulations with fracture. I. Method and tests. *Icarus* **107**, 98–116 (1994).
15. Jutzi, M., Holsapple, K., Wünneman, K. & Michel, P. in *Asteroids IV* (eds Michel, P. et al.) 679–699 (Univ. Arizona Press, 2015).
16. Ševeček, P. et al. SPH/*N*-body simulations of small ($D=10$ km) asteroidal breakups and improved parametric relations for Monte-Carlo collisional models. *Icarus* **296**, 239–256 (2017).
17. Tillotson, J. H. *Metallic Equations of State for Hypervelocity Impact* General Atomic Report GA-3216 (General Dynamics, 1962).
18. von Mises, R. Mechanik der festen Körper in plastisch-deformablen Zustand. *Nachr. d. Kgl. Ges. Wiss. Göttingen, Math.-phys. Klasse* **4**, 582–592 (1913).
19. Grady, D. & Kipp, M. Continuum modelling of explosive fracture in oil shale. *Int. J. Rock Mech. Min. Sci.* **17**, 147–157 (1980).
20. Barnes, J. & Hut, P. A hierarchical O(*N* log *N*) force-calculation algorithm. *Nature* **324**, 446–449 (1986).
21. Michel, P., Benz, W., Tanga, P. & Richardson, D. C. Collisions and gravitational reaccumulation: forming asteroid families and satellites. *Science* **294**, 1696–1700 (2001).
22. Tanga, P., Hestroffer, D., Delbo, M. & Richardson, D. C. Asteroid rotation and shapes from numerical simulations of gravitational re-accumulation. *Planet. Space Sci.* **57**, 193–200 (2009).
23. Melosh, H. J. & Ivanov, B. A. Impact crater collapse. *Ann. Rev. Earth Planet. Sci.* **27**, 385–415 (1999).
24. Riller, U. et al. Rock fluidization during peak-ring formation of large impact structures. *Nature* **562**, 511–518 (2018).
25. Jutzi, M., Asphaug, E., Gillet, P., Barrat, J.-A. & Benz, W. The structure of the asteroid 4 Vesta as revealed by models of planet-scale collisions. *Nature* **494**, 207–210 (2013).
26. Wadell, H. Volume, shape and roundness of quartz particles. *J. Geol.* **43**, 250–280 (1935).
27. Warner, B. D., Harris, A. W. & Pravec, P. The asteroid lightcurve database. *Icarus* **202**, 134–146 (2009).
28. Jehin, E. et al. TRAPPIST: TRAnsiting Planets and PlanetesImals Small Telescope. *Messenger* **145**, 2–6 (2011).
29. Pettengill, G. H., Ford, P. G., Johnson, W. T. K., Raney, R. K. & Soderblom, L. A. Magellan: radar performance and data products. *Science* **252**, 260–265 (1991).
30. Thomas, P. C. et al. The shape of Gaspra. *Icarus* **107**, 23–36 (1994).
31. Hudson, R. S. et al. *Asteroid Radar Shape Models, 6489 Golevka* PDS ID EAR-A-5-DDR-RADARSHAPE-MODELS-V1.1:RSHAPES-6489GOLEVKA-200006 (NASA PDS, 2000).
32. Ostro, S. J. et al. *Asteroid Radar Shape Models, 1620 Geographos* PDS ID EAR-A-5-DDR-RADARSHAPE-MODELS-V1.1:RSHAPES-1620GEOGRAPHOS-200006 (NASA PDS, 2000).
33. Smith, D. E. et al. Mars Orbiter Laser Altimeter: experiment summary after the first year of global mapping of Mars. *J. Geophys. Res.* **106**, 23689–23722 (2001).
34. Jorda, L. et al. Asteroid (2867) Steins: shape, topography and global physical properties from OSIRIS observations. *Icarus* **221**, 1089–1100 (2012).

35. Preusker, F. et al. Stereo-photogrammetrically derived topography of asteroid (4) Vesta. *Proc. American Geophysical Union, Meeting Number 93* abstr. P43E-05 (2012).
36. Jaumann, R. et al. Vesta's shape and morphology. *Science* **336**, 687–690 (2012).
37. Farnham, T. L. *Shape Model of Asteroid 21 Lutetia* PDS ID RO-A-OSINAC/OSIWAC-5-LUTETIA-SHAPE-V1.0 (NASA PDS, 2013).
38. Preusker, F. et al. Topography of Mercury: a global model from MESSENGER orbital stereo mapping. *Proc. Ninth Conference European Planetary Science Congress* Vol. 9 abstr. EPSC2014-709 (2014).
39. Preusker, F. et al. Dawn at Ceres—shape model and rotational state. *Proc. 47th Lunar and Planetary Science Conference* 1954 (LPI, 2016).
40. Viikinkoski, M. et al. (16) Psyche: a mesosiderite-like asteroid? *Astron. Astrophys.* **619**, L3 (2018).
41. Hanuš, J. et al. The shape of (7) Iris as evidence of an ancient large impact? *Astron. Astrophys.* **624**, A121 (2019).
42. Hiesinger, H. et al. Cratering on Ceres: implications for its crust and evolution. *Science* **353**, aaf4759 (2016).
43. Bland, M. T. et al. Composition and structure of the shallow subsurface of Ceres revealed by crater morphology. *Nat. Geosci.* **9**, 538–542 (2016).
44. Knezevic, Z. & Milani, A. Proper element catalogs and asteroid families. *Astron. Astrophys.* **403**, 1165–1173 (2003).
45. Zappala, V., Cellino, A., Farinella, P. & Milani, A. Asteroid families. II. Extension to unnumbered multiopposition asteroids. *Astron. J.* **107**, 772–801 (1994).
46. Ivezic, Ž. et al. Solar System objects observed in the Sloan Digital Sky Survey commissioning data. *Astron. J.* **122**, 2749–2784 (2001).
47. Nugent, C. R. et al. NEOWISE Reactivation Mission Year One: preliminary asteroid diameters and albedos. *Astrophys. J.* **814**, 117 (2015).
48. Usui, F. et al. Asteroid catalog using AKARI: AKARI/IRC Mid-infrared Asteroid Survey. *Pub. Astron. Soc. Jpn* **63**, 1117–1138 (2011).
49. Schäfer, C. et al. A smooth particle hydrodynamics code to model collisions between solid, self-gravitating objects. *Astron. Astrophys.* **590**, A19 (2016).
50. Collins, G. S., Melosh, H. J. & Ivanov, B. A. Modeling damage and deformation in impact simulations. *Met. Planet. Sci.* **39**, 217–231 (2004).
51. Silber, E. A., Osinski, G. R., Johnson, B. C. & Grieve, R. A. F. Effect of impact velocity and acoustic fluidization on the simple-to-complex transition of lunar craters. *J. Geophys. Res. Planets* **122**, 800–821 (2017).

Acknowledgements

P.V., A.D. and B.C. were supported by CNRS/INSU/PNP. M.Brož was supported by grant 18-04514J of the Czech Science Foundation. J.H. and J.D. were supported by grant 18-09470S of the Czech Science Foundation and by the Charles University Research Programme no. UNCE/SCI/023. This project has received funding from the European Union's Horizon 2020 research and innovation programmes under grant agreement nos 730890 and 687378. This material reflects only the authors' views, and the European Commission is not liable for any use that may be made of the information contained herein. TRAPPIST-North is a project funded by the University of Liège, in collaboration with Cadi Ayyad University of Marrakech (Morocco). TRAPPIST-South is a project funded by the Belgian Fonds (National) de la Recherche Scientifique (F.R.S.-FNRS) under grant FRFC 2.5.594.09.F. E.J. and M.G. are F.R.S.-FNRS Senior Research Associates.

Author contributions

P.V. designed the research. P.V., M.M., R.F. and T.F. reduced and deconvolved the SPHERE images. M.V. and J.H. reconstructed the 3D shape of Hygiea. L.J. and P.V. performed the analysis of Hygiea's shape. P.Š. and M.Brož ran the SPH simulations. M.F. and E.J. acquired and reduced the TRAPPIST data. M.M. and L.J. produced the albedo map. P.V. and F.D. served as principal investigators to acquire the near-infrared spectral data. B.C. provided the mass estimate. P.V., L.J., P.Š. and M.Brož worked jointly to write the manuscript. All authors discussed the results and commented on the manuscript.

Competing interests

The authors declare no competing interests.

Additional information

Supplementary information is available for this paper at https://doi.org/10.1038/s41550-019-0915-8.

Correspondence and requests for materials should be addressed to P.V.

Peer review information *Nature Astronomy* thanks Derek Richardson and the other, anonymous, reviewer(s) for their contribution to the peer review of this work.